Volume nanogratings inscribed by ultrafast IR laser in alumino-borosilicate glasses

Research Article | Vol. 31, No. 10 / 8 May 2023 / Optics Express 15449
Optics EXPRESS

Volume nanogratings inscribed by ultrafast IR laser in alumino-borosilicate glasses

HENG YAO,[1,2] QIONG XIE,[2,5] MAXIME CAVILLON,[2] DANIEL R. NEUVILLE,[3] DIEGO PUGLIESE,[4] DAVIDE JANNER,[4] YE DAI,[1,6] BERTRAND POUMELLEC,[2] AND MATTHIEU LANCRY[2]

[1]*Department of Physics, Shanghai University, 200444 Shanghai, China*
[2]*Institut de Chimie Moléculaire et des Matériaux d'Orsay, CNRS, Université Paris-Saclay, 91400 Orsay, France*
[3]*Géomatériaux, IPGP-CNRS, Université de Paris, 75005 Paris, France*
[4]*Department of Applied Science and Technology (DISAT) and RU INSTM, Politecnico di Torino, 10129 Torino, Italy*
[5]*qiong.xie@universite-paris-saclay.fr*
[6]*yedai@shu.edu.cn*

Abstract: Self-assembled nanogratings, inscribed by femtosecond laser writing in volume, are demonstrated in multicomponent alkali and alkaline earth containing alumino-borosilicate glasses. The laser beam pulse duration, pulse energy, and polarization, were varied to probe the nanogratings existence as a function of laser parameters. Moreover, laser-polarization dependent form birefringence, characteristic of nanogratings, was monitored through retardance measurements using polarized light microscopy. Glass composition was found to drastically impact the formation of nanogratings. For a sodium alumino-borosilicate glass, a maximum retardance of 168 nm (at 800 fs and 1000 nJ) could be measured. The effect of composition is discussed based on SiO_2 content, B_2O_3/Al_2O_3 ratio, and the Type II processing window is found to decrease as both $(Na_2O + CaO)/Al_2O_3$ and B_2O_3/Al_2O_3 ratios increase. Finally, an interpretation in the ability to form nanogratings from a glass viscosity viewpoint, and its dependency with respect to the temperature, is demonstrated. This work is brought into comparison with previously published data on commercial glasses, which further indicates the strong link between nanogratings formation, glass chemistry, and viscosity.

1. Introduction

In recent years, femtosecond (fs) laser direct writing (FLDW) has been a tool of choice to inscribe photo-induced transformations inside or at the surface of transparent media, including glass [1–3]. By enabling light intensities of several TW/cm^2 at the laser focal point, permanent and localized modifications within a few μm^3 of the material are possible. They are a function of both glass composition and laser parameters and have commonly been observed in silicate glasses. These include refractive index changes, micro-voids, or laser polarization dependent birefringence [4–6]. This birefringence originates from the formation of nanogratings (NGs) [7], which are made of self-aligned porous nanolayers.

Several mechanisms of the NGs formation have been proposed [7–10]. Most recently, the formation of the nanopores composing the NGs has been suggested to come from a tensile stress-assisted nano-cavitation, building on the theory developed by Grady on spall fracture of matter [11,12]. While investigating the underlying mechanisms is still an active research field, several intriguing properties arising from these structures have already been demonstrated, including, but not limited to, anisotropic light scattering [13], highly selective chemical etching [3], and form birefringence with extraordinary thermal stability [14]. In terms of applications, fabrication of polarization sensitive optical elements has been demonstrated [6], along with

#488249 https://doi.org/10.1364/OE.488249
Journal © 2023 Received 20 Feb 2023; revised 6 Apr 2023; accepted 10 Apr 2023; published 24 Apr 2023

Optics EXPRESS

ultra-stable 5-dimensional (5D) optical memory [15,16], micro/nanofluidics [3] or 3D space variant birefringent optical devices. Until now, these NGs, induced by fs-laser in volume, have been observed in various glasses and crystals including SiO_2 (by far the most studied), GeO_2 glass, TeO_2 single crystal, sapphire, Al_2O_3-Dy_2O_3 binary glass, lithium niobium silicate glass [17–23], titanium silicate glasses (ULE, Corning) [24], and even in multicomponent alumino-borosilicate glasses (Borofloat 33, Schott) [24], or barium gallo-germanate (BGG) glasses [6]. It must be pointed out that there exist multiple types of NGs, including porous NGs, crystal/glass phase separated NGs, or crack-like nanostructures. While in this work we focus on the porous NGs typically encountered in silicate or silica-rich glasses, an interested reader can find more details on the various NG types, and associated references, in [25].

Within the above list, the alumino-borosilicate glass family is particularly attractive for its excellent chemical durability, high thermal shock resistance, and low coefficient of thermal expansion. Those properties are of interest in multiple industrial applications such as liquid crystal display substrates [26] and glass fiber-reinforced polymer matrix composites [27]. Complementarily, and with respect to the present work, calcium aluminosilicate (CAS) glasses with large transmission in infrared (IR) are also of interest for a wide variety of applications, ranging from IR domes to laser windows or optical glasses [28–30]. From the discussion above, the ability to master photo-induced transformations in these glass families would therefore be a key asset in developing photonic-based devices.

In this paper, the NGs formation in a series of alumino-borosilicate doped with alkali (Na^+) and alkaline earth (Ca^{2+}) elements, respectively SAN and SAC families, is investigated. More specifically, the study focuses on the effect of composition and glass properties, such as viscosity, which can affect the overall formation of NGs. In order to tackle the latter aspects, NGs were inscribed in alumino-borosilicate glasses by varying a set of laser parameters (pulse duration and energy). Measurements of retardance (R) (see Section 2.2) and polarization dependent birefringence were performed using polarized optical microscopy, as these features indicate the presence of NGs in the glasses. The NGs processing window, defined as the ability to form NGs in a pulse energy - duration landscape, was studied according to the $(Na_2O + CaO)/Al_2O_3$ and B_2O_3/Al_2O_3 ratios. The results are then discussed on the basis of previous work revealing the key role of viscosity (η) in the formation of NGs inside several commercial glasses [11,12].

2. Experimental section

2.1. Glass synthesis and characterization

All glasses were fabricated by melting the appropriate quantities of batch precursor powders, i.e., Al_2O_3, $CaCO_3$, B_2O_3, Na_2CO_3 and SiO_2. For example, a mixture of $CaCO_3$-Al_2O_3-B_2O_3-$NaCO_3$-SiO_2 was crushed and homogenized for 1 h in alcohol using an agate mortar. Following this, the mixture was heated up slowly and progressively to decompose the carbonates, and up to the melting point. This heating process was repeated 3 times to ensure a good glass homogeneity. The studied glass compositions are presented in Table 1. Glasses are labeled according to their chemical compositions, and as follows: SAN x-y-z, with $x = SiO_2$, $y = Al_2O_3$, $z = Na_2O$ and $B_2O_3 = 100 - (x + y + z)$; SAC x-y-z with $x = SiO_2$, $y = Al_2O_3$, $z = CaO$ and $B_2O_3 = 100 - (x + y + z)$; SACN x-y-z-w with $x = SiO_2$, $y = Al_2O_3$, $z = CaO$, $w = Na_2O$ and $B_2O_3 = 100 - (x + y + z + w)$. It is worthwhile highlighting that x, y, z and w refer only to the integer part of the compositions in mol%. Additional typical values of the fabricated glasses, including glass annealing temperature (T_a), density, refractive index, and oxide/element ratios, are also provided in Table 1. The density values were obtained from the average of more than 20 measurements per sample using Archimedes' method by immerging a glass chunk in diethyl phthalate at room temperature on a Precisa XT220A weighing scale. The refractive index (n_d, at 532 nm) values were determined by the Brewster angle method.

Optics EXPRESS

Table 1. Label and batch composition of the alumino-borosilicate glasses employed in this study, along with typical physical characteristics and composition ratios.

Sample	Composition (in mol%)	Density (g/cm^3)	T_a (°C)	n_{532} (±0.005)	$\frac{Na_2O+CaO}{Al_2O_3}$	$\frac{B_2O_3}{Al_2O_3}$
SAN 75-0-12	$75SiO_2$ - $12.5B_2O_3$ - $12.5Na_2O$	2.313	570.6	1.487	No Al	No Al
SAN 75-3-12	$75SiO_2$ - $3.125Al_2O_3$ - $9.375B_2O_3$ - $12.5Na_2O$	2.354	591.7	1.493	4	3
SAN 75-6-12	$75SiO_2$ - $6.25Al_2O_3$ - $6.25B_2O_3$ - $12.5Na_2O$	2.370	618.4	1.492	2	1
SAN 75-9-12	$75SiO_2$ - $9.375Al_2O_3$ - $3.125B_2O_3$ - $12.5Na_2O$	2.386	658.2	1.491	1.33	0.33
SAN 75-12-12	$75SiO_2$ - $12.5Al_2O_3$ - $12.5Na_2O$	2.391	849.8	1.487	1	0
SAC 50-25-25	$50SiO_2$ - $25Al_2O_3$ - $25CaO$	2.624	774.7	1.566	1	0
SAC 50-12-25	$50SiO_2$ - $12.5Al_2O_3$ - $12.5B_2O_3$ - $25CaO$	2.575	700.8	1.570	2	1
SAC 50-18-25	$50SiO_2$ - $18.75Al_2O_3$ - $6.25B_2O_3$ - $25CaO$	2.566	651.9	1.559	1.33	0.33
SACN 50-6-25-5	$50SiO_2$ - $6Al_2O_3$ - $14B_2O_3$ - $25CaO$ - $5Na_2O$	2.610	667.8	1.581	5	2.33
SACN 50-12-25-5	$50SiO_2$ - $12Al_2O_3$ - $8B_2O_3$ - $25CaO$ - $5Na_2O$	2.600	689.7	1.569	2.5	0.67

2.2. Fs-laser irradiation and characterization of laser-induced modified regions

Each sample was double side polished to an optical grade prior to being irradiated by fs laser (Satsuma, Amplitude Systèmes Ltd. Pessac, France). The latter delivers pulses centered at a wavelength of 1030 nm, with a repetition rate set at 100 kHz and with varied pulse durations τ from 250 to 1500 fs. The beam was focused 500 µm below the surface (in air) using a 0.6 numerical aperture (NA) aspheric lens. The beam waist radius was estimated to be around ω_0 ~1.5 µm. The selected irradiation patterns in all samples were rectangular shapes of 10×100 µm^2 dimensions. In fact, each rectangle is composed of a set of 10 lines spaced out by $\Delta y = 1$ µm, to get a homogenous irradiated area and avoid any diffraction effect. To favor NGs formation a writing speed of 10 µm/s was used, therefore translating into a pulse density of 10,000 pulses/µm (at 100 kHz), which is a typical value to induce NGs [31]. Moreover, the pulse energy E_p was varied from 0.025 to 3 µJ and two laser polarization configurations were tested, namely "Xx" and "Xy" (X being the laser writing orientation and x, y the laser polarization orientation at 0 and 90° relative to X, respectively) [32]. After fs laser irradiation, the inscribed samples were observed using a polarizing optical microscope (Olympus BX60, Tokyo, Japan) equipped with a high precision quarter waveplate coupled to a rotating analyzer providing a quantitative measurement of R [32]. The R is defined by $R = B \times l$, where B is linear birefringence and l the thickness of the birefringent layer. Such R measurements coupled to slow axis measurements enable one to elucidate the formation of NGs since these structures are both birefringent and oriented by the writing laser polarization.

3. Results

3.1. Optical modifications in the pulse energy - pulse duration landscape

It has been reported that the R detection threshold (characteristic of NGs formation) strongly depends on the laser light intensity for all alkali-free alumino-borosilicate (AF32), multicomponent borosilicate (Borofloat33) and silica glasses [33]. Such threshold is thus a function of the ratio of pulse energy to the pulse duration. The threshold was found to be slightly above 1 TW/cm^2 for AF32 and silica glasses [33,34]. Therefore, the pulse energy - duration landscape is a key point to evaluate the formation of NGs, and therefore was chosen herein. On other hand, the dependence of colouration and scattering to "Type II-like" on the pulse duration has been reported in [13,35]. While probing this landscape, several types of transformations, typically found in most oxide glasses, are revealed. The observed permanent modifications are classified as Type I, Type II, and what we have called "spatial broadening regime". Type I corresponds to an isotropic refractive index change leading to a permanent contrast in non-polarized optical microscopy

Optics EXPRESS

which can be further quantified in optical phase microscopy. Type II corresponds to the NGs regime and is identified as the observation of a birefringence response from the irradiated area whose orientation depends on the writing laser polarization. This is usually identified as form birefringence due to NGs formation [6] and can be observed with polarized light microscopy equipped with a full retardation waveplate. A last type of modification appearing at high laser intensities can be finally defined. Often imprecisely called "heat accumulation regime" in the literature, this modification corresponds to a smooth and homogeneous variation of the refractive index with a tendency of laser tracks to become much larger than the laser beam size. This spatially broadened "Type I-like" modification will therefore be referred to as "spatial broadening regime", which describes more accurately this phenomenon [4].

In the following we will study 3 glass families, namely SAN, SAC and SACN, which exhibit different chemical composition and stoichiometry. At first SAC 50-25-25 glass was selected since its composition contains both no boron and the highest amount of Al_2O_3, which is equal to the amount of CaO, and with the minimum ratio of $(Na_2O + CaO)/Al_2O_3$. Figure 1 summarizes the three different fs laser-induced transformations for such SAC 50-25-25 glass at a fixed repetition

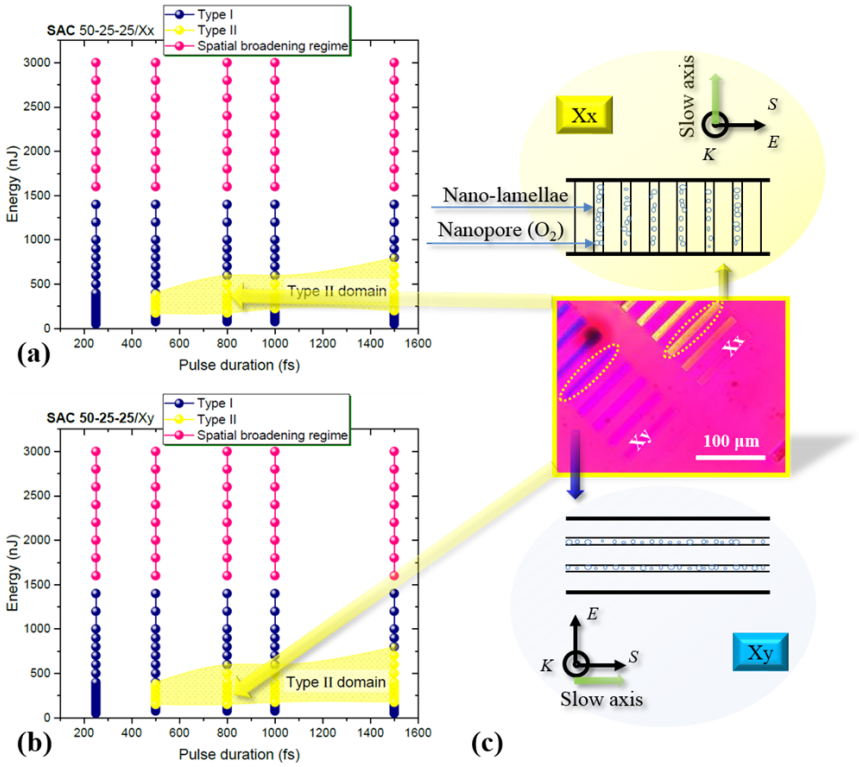

Fig. 1. Laser-induced modifications in pulse energy - duration landscape. Transformation regimes encountered in the experimental conditions: Type I, Type II and spatial broadening regime. The selected sample is SAC 50-25-25 with Xx (a) and Xy (b) writing polarization configurations, respectively. (c) Sketch of two configurations of fs laser induced NGs with the corresponding orientations of slow axis indicated in bulk glass. Inset shows the polarized optical microscope image (bottom light illumination) with crossed polarizers and a full waveplate inserted at 45°. *E*: laser polarization direction, *K*: laser beam propagation direction and *S*: laser scanning direction. Laser parameters: 1030 nm, 0.6 NA, 100 kHz, 10 µm/s.

Optics EXPRESS

rate of 100 kHz and is intended to illustrate the observed features, which are common to all investigated glasses, although in varying proportions.

As shown in Fig. 1(a) and (b), our results indicate that SAC 50-25-25 glass irradiated with both Xx and Xy configurations [32] possesses broad energy windows both for Type I (from 25 to 1400 nJ) and spatial broadening regime (from 1600 up to 3000 nJ). Furthermore, there are no NGs detected at 250 fs inside SAC 50-25-25 glass, confirming that shorter pulse durations are disadvantageous for the NGs formation in agreement with the literature [33,34,36,37], which may be related to a limitation in terms of plasma density that is not high enough to initiate the nanopores formation. Then for pulse durations above 500 fs, a Type II processing window appears as revealed by comparing Xx and Xy writing configurations. The typical sketch of these two configurations including nanolayers and the formed O_2-contaning nanopores (usually seen by Raman spectroscopy), is illustrated in Fig. 1(c), in which a polarized optical microscope image with a first order full waveplate inserted is provided. This enables the identification of the slow axis (indicated in Fig. 1(c)) of the laser tracks and its 90° rotation when switching the polarization from x to y in the reference frame, indicative of the existence of Type II modifications. Finally, a slight increase of Type II window width for longer pulse durations was observed, in agreement with Ref. [6]. This is likely related to a lower peak power leading to a less efficient overall absorption by the free electron plasma in relatively long pulse duration, in agreement with recent results reported for silica glass [38], e.g. the absorbed energy was 95 nJ for 300 fs at pulse energy of 690 nJ, while the absorbed energy was 17 nJ for 500 fs at the equivalent pulse energy.

Interestingly, the Type I regime, as previously described, is found to reappear as the energy is progressively increased and while the Type II window collapses. This feature suggests that there is likely a combination / overlap of Type I and Type II domains, which can imply several hypotheses such as i) the material in-between the porous nanolayers is likely a kind of Type I modification and ii) at high energies the nanopores are likely erased after the energy deposition and during the resulting heating-cooling process [31].

3.2. *Effect of the chemical composition on the optical retardance and Type II energy window*

It has previously been established that the deposited energy, pulse duration, and writing configurations are key parameters that impact on the formation of NGs in oxide glasses [6,38]. To study such effects, the dependence of the optical retardance, R, on these factors has been quantitatively investigated. Firstly, quantitative R results obtained in the SAC 50-25-25 glass at different pulse durations are highlighted in Fig. 2(a), as it serves, as before, as an exemplar throughout this work. Above a threshold of around 100-150 nJ, the overall R increases up to a maximum, and then strongly decreases as the energy is continuously increased. The latter part corresponds to the formation of inhomogeneous and disrupted NGs that can be assigned to a significant temperature increase at higher pulse energies [39,40]. Finally, no polarization dependent birefringence, required to confirm the presence of NGs, could be observed above a certain energy value.

Secondly, it was also found that for a given glass the maximum R tends to saturate for all investigated pulse durations (and for both Xx and Xy configurations). It is then followed by a decrease for longer pulse durations (e.g., 1500 fs in Xx configuration). This quantitative increase of R can be simply explained by an elongated focal spot yielding to longer laser tracks. In contrast, the decrease for longer pulse duration might be related to some thermal effects in the picosecond regime that affect the nanopores size and filling factor [41], due to the lower melting point of alumino-borosilicate glasses.

Finally, higher R values are measured in Xx configuration compared to the Xy one, as shown in Fig. 2(a) and (b), due to the combined effect of stress-induced birefringence around nano-lamellae, as previously reported [42]. This is particularly visible in the SAC 50-25-25 glass case at 800

Optics EXPRESS

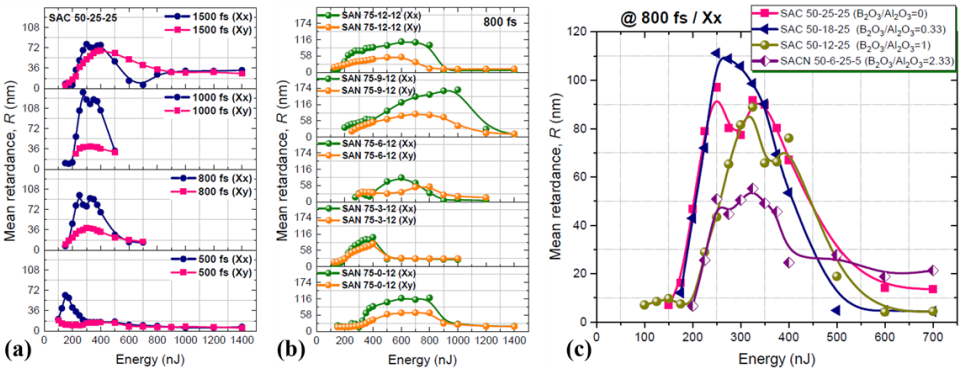

Fig. 2. Mean retardance, *R*, of laser-written structures as a function of pulse energy for (a) SAC 50-25-25 glass with pulse durations of 500, 800, 1000 and 1500 fs, using Xx and Xy configurations, (b) a series of SAN glasses at 800 fs using Xx and Xy configurations, (c) SAC 50-25-25, SAC 50-18-25, SAC 50-12-25 and SACN 50-6-25-5 glasses at 800 fs using Xx configuration.

and 1000 fs, for which the maximum *R* (i.e., 97 nm at 800 fs and 136 nm at 1000 fs) of Xx configuration was 2.5 and 3.4 times higher than that of Xy configuration at 800 fs (i.e., 39 nm) and 1000 fs (i.e., 40 nm), respectively.

To continue investigating the NGs processing windows and the effect of boron/aluminum oxides in the presence of alkali, the results of the SAN glass series were investigated. The *R* values, for a fixed 800 fs laser pulse duration, and for varying pulse energy values, are shown in Fig. 2(b). These alkali-containing glasses showed a wide range of *R* values, strongly dependent on glass composition, pulse energy, and polarization (Xx and Xy configuration). In the SAN family glasses, the maximum *R* (168 nm) was measured in the SAN 75-9-12 glass sample having an Xx writing configuration and at 1000 nJ, where the ratio B_2O_3/Al_2O_3 is equal to 0.33 (see Table 1).

As previously investigated and stated, both Xx configuration and 800 fs pulse duration were found to be optimized parameters, within the context of this study, to imprint high *R* NGs (Fig. 2(a) and (b)). Therefore, the calcium-containing glass series was investigated by keeping these two parameters fixed, and the results of *R* as a function of pulse energy are reported in Fig. 2(c). SAC 50-25-25 glass (i.e., B_2O_3-free glass) is first compared to the two SAC glasses, where B_2O_3 is added. Then, the three aforementioned glasses are compared to the SACN 50-6-25-5 glass, which contains both alkali (Na^+) and alkaline earth (Ca^{2+}) cations (as opposed to only Ca^{2+} cations). It is found that the minimum pulse energy required to induce detectable *R* was in the range of 100-150 nJ and it increased slightly when increasing the B_2O_3/Al_2O_3 ratio. Overall, SAC 50-18-25 glass, which owns the lowest B_2O_3/Al_2O_3 ratio of 0.33, showed a maximum *R* value of 110 nm at 250 nJ. It can be explained that the viscosity (impacted by chemical composition) and created free plasma density are in optimized state to obtain the maximum optical retardance. This needs further investigations. Interestingly, higher *R* values were measured in SAN 75-9-12 and SAN 75-12-12 glasses compared to the calcium containing glasses, as shown in (b). In addition, the *R* decreased as the alkali metal (Na^+) content increased, e.g., SACN 50-6-25-5 glass (see Fig. 2(c)). In short, the effect of sodium seems drastic probably due to Na^+ chemical migration, and the results obtained on the B/Al mixture in SACs are in the same direction as the results for SANs. While this effect requires further investigations to be clarified, this agrees with the literature, which reported on the detrimental effect of Na_2O for NGs formation in SiO_2-Na_2O [43] and GeO_2-Na_2O [44] glasses.

Optics EXPRESS

4. Discussion and rationalization

4.1. Key role played by the viscosity on Type II energy window

The domain of existence of the nanopores (and thus NGs) can be anticipated by using a simple approach following viscosity-based arguments [11,12]. In order to investigate this aspect, the viscosity profiles as a function of temperature and the estimated domain of NGs existence are reported in Fig. 3(a) for all the oxide glasses investigated in this work. Here the investigated glass viscosities were modeled using SciGlass software and the obtained data as a function of temperature were subsequently fitted using the Vogel–Fulcher–Tammann (VFT) equation [45].

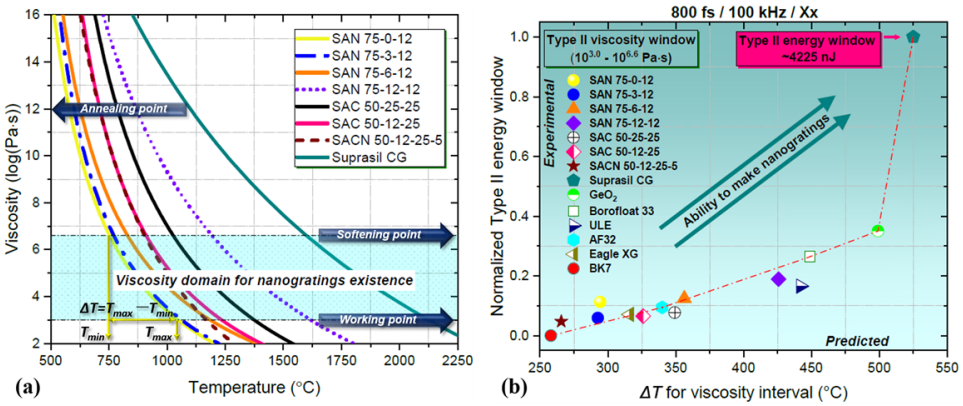

Fig. 3. (a) Viscosity as a function of temperature for a variety of alumino-borosilicate and SiO_2 (Suprasil CG, taken as a reference) glasses, along with an estimated domain of NGs existence from T_{min} ($\eta = 10^{6.6}$ Pa·s, i.e., softening temperature) to T_{max} ($\eta = 10^{3.0}$ Pa·s, working temperature). (b) Normalized Type II energy window vs. temperature interval ($\Delta T = T_{max}$ - T_{min}) for a variety of alumino-borosilicate and commercial glasses. The x axis presents the predicted results of temperature interval from (a) and the y axis presents the experimental results.

The domain of NGs existence was predicted by considering two boundaries [11] in terms of viscosity, which can then be translated into two limiting temperatures. The lower limit corresponds to the temperature, $T_{min} = T_{soft}$, i.e., softening temperature, at which nanocavitation in the glass can occur and for which the viscosity value (η) is situated at around $\sim 10^{6.6}$ Pa·s, forming nanopores that compose the NGs. The upper temperature limit, $T_{max} = T_{working}$, i.e., working temperature, relates to either the collapse or unstable hydrodynamic growth of the nanopores, resulting in the disappearance of the nanopores, hence the NGs structuring. This corresponds to a viscosity value typically around $\sim 10^{3.0}$ Pa·s, i.e., the so-called working temperature of glass, and was determined using the Peclet number (ratio between the viscous deformation and thermal diffusion rate) as a local indicator for nanopores erasure [46]. The broadness of NGs existence window (i.e. its extent in terms of pulse energy), was then estimated by considering the temperature interval (ΔT) between T_{max} and T_{min} as previously defined. The upper and lower boundaries of the viscosity corresponding to the T_{min} / T_{max} interval, are provided in Fig. 3(a). Note that $\eta = 10^{12.0}$ Pa·s, also reported in the figure, corresponds to the annealing temperature and is given for completeness. The temperature interval (ΔT) was calculated for each glass and reported on the x-axis of Fig. 3(b). On the y-axis is reported the Type II energy window, calculated by taking the extent of the Type II window in the pulse energy - duration landscape, and subsequently normalized relatively to SiO_2 (set as 1), i.e. $(E_{max(glass)} - E_{min(glass)})/(E_{max} - E_{min})$ where $E_{max(glass)}$ and $E_{min(glass)}$ present the energies to NGs collapsed and formed for the corresponding glass studied, respectively. The E_{max} and E_{min} are respectively energies of SiO_2 glass. ΔT is progressively enlarging for glasses

Optics EXPRESS

in the following order: SAN 75-12-12 > SAN 75-6-12 > SAC 50-25-25 > SAC 50-12-25 > SAN 75-0-12 ≈ SAN 75-3-12 > SACN 50-12-25-5. On average, the normalized Type II window extent (normalized with respect to silica) monotonously increased with ΔT at a slope of 0.0015 $°C^{-1}$ for the alumino-borosilicate glasses and the commercial glasses apart from SiO_2 (Suprasil CG), which exhibited the broadest Type II window and a higher slope of 0.025 $°C^{-1}$ (the slope from GeO_2 to SiO_2). The viscosity modeling results were basically in agreement with experimental data, further supporting and confirming the viscosity (η) role on the NGs formation, recently suggested [11]. As a general view, glasses with low Si and high (alkali + alkaline earth) content possess low network connectivity and relatively abundant non-bridging oxygens (NBOs) [47,48]. This will further lead to lower viscosity of the glass, e.g., the viscosity of SAN 75-12-12 is higher than that of SAC 50-12-25 (low Si and high (alkali + alkaline earth) content).

4.2. Influence of the chemical composition on the Type II energy window

Type II energy window can also be studied with respect to glass composition, and more specifically relative to ratios such as $(Na_2O + CaO)/Al_2O_3$ or B_2O_3/Al_2O_3. The results are displayed in Fig. 4(a) and (b). The first, i.e., $(Na_2O + CaO)$ to Al_2O_3 ratio, distinguishes the glass compositions between peralkaline $[(Na_2O + CaO) > Al_2O_3]$ (like SAC, SACN family samples), metaluminous (like most SAN samples) and peraluminous $[Al_2O_3 > (Na_2O + CaO)]$, and is a prime factor controlling the formation of NGs. The addition of alkali and alkaline earth elements in glasses can provide strong structural changes due to the role of network modifiers, such as bond breaking and even forming some "channels" as reported for Na_2O glasses [49]. In a simple view, alkali and alkaline earth atoms play the role of depolymerizing cations (i.e., behaving as a modifying cation, breaking T-O-T linkages (T = Si, Al) and forming nonbridging ≡Si-O- bonds [50], lowering the degree of polymerization of the main structural groups and consequently decreasing the viscosity of glass (a key factor in NGs formation/erasure mechanisms [11]. Indeed, Liu *et al.* [51] reported that flow could involve the relative motion of large molecular units (e.g., chains or sheets) due to depolymerized networks. Therefore, with the decrease of the $(Na_2O + CaO)/Al_2O_3$ ratio, the network structure of glass is more rigid and connected, which might favor the formation of NGs [11]. From Fig. 4(a), the increase in $(Na_2O + CaO)/Al_2O_3$ ratio is indeed accompanied with a decrease of the Type II window (materialized by the green area and bounded by lower and upper energy limits yielding to the observation of NGs). Fernandez *et al.* [47] also reported that (alkali + alkaline earth)/Al_2O_3 ratio directly affected the viscosity, and the viscosity was at its maximum when the (alkali + alkaline earth)/Al_2O_3 ratio was 1, where in other words there was a kind of balance between Al and charge compensating modifiers. This is the case for SAN 75-12-12 glass, which correspondingly owns the largest processing window. Since Na is always more mobile than Ca, one could imagine that Ca compensates and Na makes non-bridging oxygen which could explain the behavior of Na-containing glasses (e.g. SACN).

Interestingly, although exhibiting the same $(Na_2O + CaO)/Al_2O_3$ ratio equal to 2, the two peralkaline glasses SAC 50-12-25 and SAN 75-6-12 revealed significantly different Type II windows. Na-containing alumino-borosilicate glass (SAN 75-6-12) showed a roughly 2 times broader Type II window with respect to the Ca-containing one (SAC 50-12-25). At a first sight, one could think that the higher SiO_2 content should rather lead to the opposite observation since $(Na_2O + CaO)/SiO_2$ ratio is much lower for SAN 75-6-12 glass (i.e., 12.5/75) compared to SAC 50-12-25 glass (i.e., 25/50). However, it appears clearly from the glass annealing temperatures, T_a, and the viscosity curves (see Fig. 3(a) and Table 1) that SAC 50-12-25 glass owns a higher viscosity revealing in a more rigid network structure or increased network connectivity compared to SAN 75-6-12 glass. It appears again here that the main driver for NGs formation is not simply the viscosity, but it is rather the temperature dependence of viscosity and especially its slope in the range between $\eta = 10^{6.6}$ Pa·s (softening point) and $\eta = 10^{3.0}$ Pa·s (working point) [11]. However, it is worthwhile noting that the chemical composition is one of the causes which indirectly decides

Optics EXPRESS

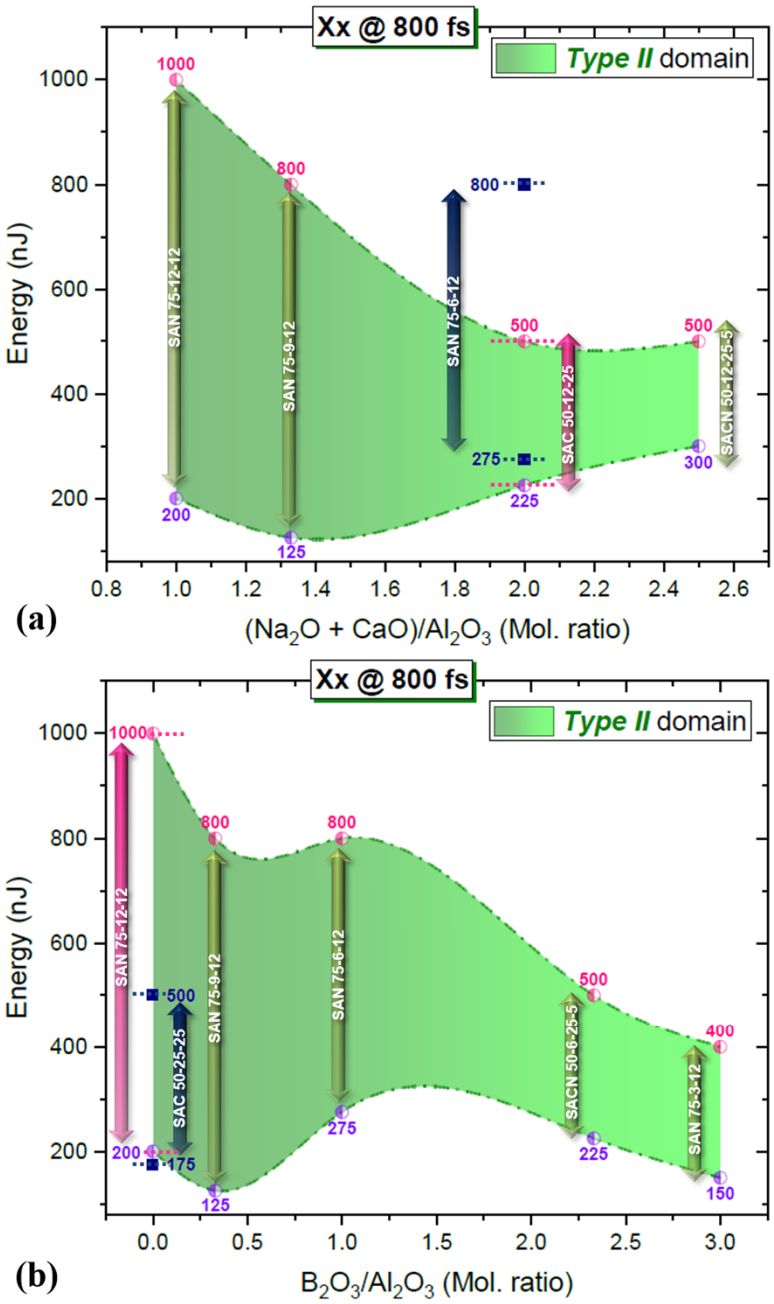

Fig. 4. Type II processing window for the different glass groups under study illustrated in a pulse energy vs. (a) $(Na_2O + CaO)/Al_2O_3$ and (b) B_2O_3/Al_2O_3 ratio landscape. The ratios are given by using glass composition in mol.%. Fixed laser parameters are: 800 fs and Xx writing configuration. The length of double head arrow indicates roughly the width of type II energy window.

Optics EXPRESS

the amplitude of viscosity of the glass. The viscosity is impacted by the network structure and, in parallel, network structure is determined by the chemical composition.

Finally, the width of the type II windows has been reported in Fig. 4(b) as a function of B_2O_3/Al_2O_3 ratio (in mol. ratio). As a general trend, the Type II window decreased while increasing the B_2O_3/Al_2O_3 ratio or along B/Al mixture. Here, the substitution of Al_2O_3 by B_2O_3 leads to a strong viscosity declining as a function of temperature, as visible from Fig. 3(a) when considering the SAN glass series. More specifically, the viscosity curves become steeper, in the $10^{6.6}$ - $10^{3.0}$ Pa·s viscosity range of interest, when increasing B_2O_3/Al_2O_3 ratio, which turns out to be detrimental for NGs formation in the framework of our model. In addition, by comparing the two glasses SAN 75-12-12 and SAC 50-25-25, which both have no Boron oxide and the same $(Na_2O + CaO)/Al_2O_3$ ratio, it is worthwhile noting that SAN 75-12-12 owns a much wider Type II processing window. This has been attributed to the different $(Na_2O + CaO)/SiO_2$ ratio, namely 12.5/75 for SAN 75-12-12 glass against the much higher value of 25/50 exhibited by the SAC 50-25-25 glass. Again, one can clearly see in Fig. 3(a) that the SAN 75-12-12 appears to be a "long glass" [11] compared to SAC 50-25-25, for which the viscosity drastically reduces at high temperature. The corresponding temperature intervals $\Delta T = T_{max}$ - T_{min} are thus estimated to be 425 °C for SAN 75-12-12 and 350 °C for SAC 50-25-25 glasses.

5. Conclusion

In summary, (alkali, alkaline earth)-doped alumino-borosilicate glasses revealed the formation of NGs by irradiation through fs laser. The upper limit of existence of NGs occurred at relatively high pulse energies (i.e., 600 nJ for SAC 50-25-25 glass), while Type I modification was observed again surpassing this energy. The maximum retardance of 168 nm was exhibited by SAN 75-9-12 glass at 800 fs and 1000 nJ, revealing that the B_2O_3/Al_2O_3 molar ratio and relatively high SiO_2 content are of primary importance in the formation of NGs. Moreover, an interpretation from the viscosity point of view is demonstrated and the normalized Type II processing windows of a series of alumino-borosilicate glasses along with the current commercial glasses vs. temperature interval are exhibited, in turn basically confirming the consistence between viscosity modeling results and experimental data. Furthermore, Type II window was found to be gradually narrower while increasing (alkali + alkaline earth)/Al_2O_3 and B_2O_3/Al_2O_3 molar ratios due to the depolymerizing network of alkali plus alkaline earth metal elements, the increased connectivity of SiO_2 network and the glass "fragility" induced by B_2O_3 doping further indicate the dependence of Type II processing window on the chemical composition.

Funding. National Natural Science Foundation of China (12274280, 11774220); Science and Technology Innovation Plan of Shanghai Science and Technology Commission (20JC1415700); China Scholarship Council; Agence Nationale de la Recherche (ANR-18-CE08-0004-01, FLAG-IR Project).

Disclosures. The authors declare no conflicts of interest.

Data availability. Data underlying the results presented in this paper are not publicly available at this time but may be obtained from the authors upon reasonable request.

References

1. L. Orazi, L. Romoli, M. Schmidt, and L. Li, "Ultrafast laser manufacturing: from physics to industrial applications," CIRP Ann. **70**(2), 543–566 (2021).
2. R. Stoian, "Volume photoinscription of glasses: three-dimensional micro- and nanostructuring with ultrashort laser pulses," Appl. Phys. A **126**(6), 438 (2020).
3. Y. Bellouard, A. Said, M. Dugan, and P. Bado, "Fabrication of high-aspect ratio, micro-fluidic channels and tunnels using femtosecond laser pulses and chemical etching," Opt. Express **12**(10), 2120–2129 (2004).
4. H. Yao, R. Zaiter, M. Cavillon, B. Sapaly, F. Calzavara, P. Delullier, T. Cardinal, Y. Dai, B. Poumellec, and M. Lancry, "Photosensitivity of barium germano-gallate glasses under femtosecond laser direct writing for Mid-IR applications," Ceram. Int. **47**(24), 34235–34241 (2021).
5. E. N. Glezer and E. Mazur, "Ultrafast-laser driven micro-explosions in transparent materials," Appl. Phys. Lett. **71**(7), 882–884 (1997).

Optics EXPRESS

6. H. Yao, R. Zaiter, M. Cavillon, P. Delullier, B. Lu, T. Cardinal, Y. Dai, B. Poumellec, and M. Lancry, "Formation of nanogratings driven by ultrafast laser irradiation in mid-IR heavy oxide glasses," Ceram. Int. **48**(21), 31363–31369 (2022).
7. Y. Shimotsuma, P. G. Kazansky, J. Qiu, and K. Hirao, "Self-organized nanogratings in glass irradiated by ultrashort light pulses," Phys. Rev. Lett. **91**(24), 247405 (2003).
8. R. Taylor, C. Hnatovsky, and E. Simova, "Applications of femtosecond laser induced self-organized planar nanocracks inside fused silica glass," Laser Photonics Rev. **2**(1-2), 26–46 (2008).
9. V. R. Bhardwaj, E. Simova, P. P. Rajeev, C. Hnatovsky, R. S. Taylor, D. M. Rayner, and P. B. Corkum, "Optically produced arrays of planar nanostructures inside fused silica," Phys. Rev. Lett. **96**(5), 057404 (2006).
10. M. Beresna, M. Gecevičius, P. G. Kazansky, T. Taylor, and A.V. Kavokin, "Exciton mediated self-organization in glass driven by ultrashort light pulses," Appl. Phys. Lett. **101**(5), 053120 (2012).
11. Q. Xie, M. Cavillon, B. Poumellec, D. Pugliese, D. Janner, and M. Lancry, "Application and validation of a viscosity approach to the existence of nanogratings in oxide glasses," Opt. Mater. **130**, 112576 (2022).
12. A. Rudenko, J. -P. Colombier, and T. E. Itina, "Nanopore-mediated ultrashort laser-induced formation and erasure of volume nanogratings in glass," Phys. Chem. Chem. Phys. **20**(8), 5887–5899 (2018).
13. M. Sakakura, Y. Lei, L. Wang, Y. -H. Yu, and P. G. Kazansky, "Ultralow-loss geometric phase and polarization shaping by ultrafast laser writing in silica glass," Light: Sci. Appl. **9**(1), 15 (2020).
14. E. Bricchi and P. G. Kazansky, "Extraordinary stability of anisotropic femtosecond direct-written structures embedded in silica glass," Appl. Phys. Lett. **88**(11), 111119 (2006).
15. Y. Shimotsuma, M. Sakakura, P. G. Kazansky, M. Beresna, J. Qiu, K. Miura, and K. Hirao, "Ultrafast manipulation of self-assembled form birefringence in glass," Adv. Mater. **22**(36), 4039–4043 (2010).
16. J. Zhang, M. Gecevičius, M. Beresna, and P. G. Kazansky, "Seemingly unlimited lifetime data storage in nanostructured glass," Phys. Rev. Lett. **112**(3), 033901 (2014).
17. Y. Shimotsuma, T. Asai, M. Sakakura, and K. Miura, "Femtosecond-laser nanostructuring in glass," J. Laser Micro/Nanoeng. **9**(1), 31–36 (2014).
18. F. Zhang, H. Zhang, G. Dong, and J. Qiu, "Embedded nanogratings in germanium dioxide glass induced by femtosecond laser direct writing," J. Opt. Soc. Am. B **31**(4), 860–864 (2014).
19. T. Asai, Y. Shimotsuma, T. Kurita, A. Murata, S. Kubota, M. Sakakura, K. Miura, F. Brisset, B. Poumellec, and M. Lancry, "Systematical control of structural changes in GeO_2 glass induced by femtosecond laser direct writing," J. Am. Ceram. Soc. **98**(5), 1471–1477 (2015).
20. Y. Shimotsuma, K. Hirao, J. Qiu, and P. G. Kazansky, "Nano-modification inside transparent materials by femtosecond laser single beam," Mod. Phys. Lett. B **19**(05), 225–238 (2005).
21. Q. Zhai, H. Ma, X. Lin, Y. Li, W. Yin, X. Tang, X. Zeng, and Y. Dai, "Evolution of self-organized nanograting from the pre-induced nanocrack-assisted plasma–laser coupling in sapphire," Appl. Phys. B **127**(5), 74 (2021).
22. Y. Shimotsuma, S. Mori, Y. Nakanishii, E. Kim, M. Sakakura, and K. Miura, "Self-assembled glass/crystal periodic nanostructure in Al_2O_3-Dy_2O_3 binary glass," Appl. Phys. A **124**(1), 82 (2018).
23. J. Cao, L. Mazerolles, M. Lancry, F. Brisset, and B. Poumellec, "Modifications in lithium niobium silicate glass by femtosecond laser direct writing: morphology, crystallization, and nanostructure," J. Opt. Soc. Am. B **34**(1), 160–168 (2017).
24. S. Richer, C. Miese, S. Döring, F. Zimmermann, M. J. Withford, A. Tünnermann, and S. Notle, "Laser induced nanogratings beyond fused silica - periodic nanostructures in borosilicate glasses and ULE^{TM}," Opt. Mater. Express **3**(8), 1161–1166 (2013).
25. B. Poumellec, M. Cavillon, and M. Lancry, "Electrostatic interpretation of phase separation induced by femtosecond laser light in glass," Crystals **13**(3), 393 (2023).
26. A. Ellison and I. A. Cornejo, "Glass substrates for liquid crystal displays," Int. J. Appl. Glass Sci. **1**(1), 87–103 (2010).
27. F. T. Wallenberger, "The effects of lithia and alumina on the viscosity and strength of commercial fibreglass and other glass compositions," Glass Technol.: Eur. J. Glass Sci. Technol., Part A **52**(4), 117–126 (2011).
28. M. E. Lines, J. B. MacChesney, K. B. Lyons, A. J. Bruce, A. E. Miller, and K. Nassau, "Calcium aluminate glasses as potential ultralow-loss optical materials at 1.5–1.9 μm," J. Non-Cryst. Solids **107**(2-3), 251–260 (1989).
29. L. -G. Hwa, S. -L. Hwang, and L. -C. Liu, "Infrared and Raman spectra of calcium alumino-silicate glasses," J. Non-Cryst. Solids **238**(3), 193–197 (1998).
30. F. T. Wallenberger, R. J. Hicks, and A. T. Bierhals, "Design of environmentally friendly fiberglass compositions: ternary eutectic SiO_2–Al_2O_3–CaO compositions, structures and properties," J. Non-Cryst. Solids **349**, 377–387 (2004).
31. Q. Xie, M. Cavillon, D. Pugliese, D. Janner, B. Poumellec, and M. Lancry, "On the formation of nanogratings in commercial oxide glasses by femtosecond laser direct writing," Nanomaterials **12**(17), 2986 (2022).
32. J. Tian, H. Yao, M. Cavillon, E. Garcia-Caurel, R. Ossikovski, M. Stchakovsky, C. Eypert, B. Poumellec, and M. Lancry, "A comparison between nanogratings-based and stress-engineered waveplates written by femtosecond laser in silica," Micromachines **11**(2), 131 (2020).
33. S. S. Fedotov, R. Drevinskas, S. V. Lotarev, A. S. Lipatiev, M. Beresna, A. Čerkauskaitė, V. N. Sigaev, and P. G. Kazansky, "Direct writing of birefringent elements by ultrafast laser nanostructuring in multicomponent glass," Appl. Phys. Lett. **108**(7), 071905 (2016).

Optics EXPRESS

34. Y. Liao, B. Zeng, L. Qiao, L. Liu, K. Sugioka, and Y. Cheng, "Threshold effect in femtosecond laser induced nanograting formation in glass: influence of the pulse duration," Appl. Phys. A **114**(1), 223–230 (2014).
35. T. Ohfuchi, Y. Yamada, M. Sakakura, N. Fukuda, T. Takiya, Y. Shimotsuma, and K. Miura, "The Characteristic of Birefringence and Optical Loss in Femtosecond-Laser-Induced Region in terms of Nanogratings Distribution," J. Laser Micro Nanoen. **12**(3), 217–221 (2017).
36. F. Zimmermann, A. Plech, S. Richter, S. Döring, A. Tünnermann, and S. Nolte, "Structural evolution of nanopores and cracks as fundamental constituents of ultrashort pulse-induced nanogratings," Appl. Phys. A **114**(1), 75–79 (2014).
37. C. Mauclair, M. Zamfirescu, J. P. Colombier, G. Cheng, K. Mishchik, E. Audouard, and R. Stoian, "Control of ultrafast laser-induced bulk nanogratings in fused silica via pulse time envelopes," Opt. Express **20**(12), 12997–13005 (2012).
38. H. Wang, Y. Lei, L. Wang, M. Sakakura, Y. Yu, G. Shayeganrad, and P. G. Kazansky, "100-layer error-free 5D optical data storage by ultrafast laser nanostructuring in glass," Laser Photonics Rev. **16**(4), 2100563 (2022).
39. F. Zhang, A. Cerkauskaite, R. Drevinskas, P. G. Kazansky, and J. Qiu, "Microengineering of optical properties of GeO_2 glass by ultrafast laser nanostructuring," Adv. Opt. Mater. **5**(23), 1700342 (2017).
40. F. Zhang, Z. Nie, H. Huang, L. Ma, H. Tang, M. Hao, and J. Qiu, "Self-assembled three-dimensional periodic micro-nano structures in bulk quartz crystal induced by femtosecond laser pulses," Opt. Express **27**(5), 6442–6450 (2019).
41. M. Gecevičius, "Polarization sensitive optical elements by ultrafast laser nanostructuring of glass," University of Southampton, Physical Sciences and Engineering, Doctoral Thesis (2015), 197 pp.
42. M. Gecevičius, M. Beresna, J. Zhang, W. Yang, H. Takebe, and P. G. Kazansky, "Extraordinary anisotropy of ultrafast laser writing in glass," Opt. Express **21**(4), 3959–3968 (2013).
43. J. Wang, X. Liu, Y. Dai, Z. Wang, and J. Qiu, "Effect of sodium oxide content on the formation of nanogratings in germanate glass by a femtosecond laser," Opt. Express **26**(10), 12761–12768 (2018).
44. S. V. Lotarev, S. S. Fedotov, A. I. Kurina, A. S. Lipatiev, and V. N. Sigaev, "Ultrafast laser-induced nanogratings in sodium germanate glasses," Opt. Lett. **44**(7), 1564–1567 (2019).
45. D. R. Neuville, "Viscosity, structure and mixing in (Ca, Na) silicate melts," Chem. Geol. **229**(1-3), 28–41 (2006).
46. A. Rudenko, J. -P. Colombier, S. Höhm, A. Rosenfeld, J. Krüger, J. Bonse, and T. E. Itina, "Spontaneous periodic ordering on the surface and in the bulk of dielectrics irradiated by ultrafast laser: a shared electromagnetic origin," Sci. Rep. **7**(1), 12306 (2017).
47. T. T. Fernandez, S. Gross, K. Privat, B. Johnston, and M. Withford, "Designer glasses—future of photonic device platforms," Adv. Funct. Mater. **32**(3), 2103103 (2022).
48. T. T. Fernandez, M. Sakakura, S. M. Eaton, B. Sotillo, J. Siegel, J. Solis, Y. Shimotsuma, and K. Miura, "Bespoke photonic devices using ultrafast laser driven ion migration in glasses," Prog. Mater. Sci. **94**, 68–113 (2018).
49. G. S. Henderson and J. F. Stebbins, "The short-range order (SRO) and structure," Rev. Mineral. Geochem. **87**(1), 1–53 (2022).
50. D. R. Neuville, L. Cormier, and D. Massiot, "Al coordination and speciation in calcium aluminosilicate glasses: Effects of composition determined by ^{27}Al MQ-MAS NMR and Raman spectroscopy," Chem. Geol. **229**(1-3), 173–185 (2006).
51. S. -B. Liu, J. F. Stebbins, E. Schneider, and A. Pines, "Diffusive motion in alkali silicate melts: An NMR study at high temperature," Geochim. Cosmochim. Acta **52**(2), 527–538 (1988).